ISSN 0016-7037
Volume 72, Number 16
August 15, 2008

Geochimica et Cosmochimica Acta

JOURNAL OF THE GEOCHEMICAL SOCIETY AND THE METEORITICAL SOCIETY

Volume 72, Number 16 August 15, 2008

Articles

Continued on outside back cover

Available online at www.sciencedirect.com
ScienceDirect
Geochimica et Cosmochimica Acta 72 (2008) 3980–3990
Geochimica et Cosmochimica Acta
www.elsevier.com/locate/gca

Analysis of coupled Sr/Ca and $^{87}Sr/^{86}Sr$ variations in enamel using laser-ablation tandem quadrupole-multicollector ICPMS

Vincent Balter [a,*], Philippe Telouk [b], Bruno Reynard [b], José Braga [c], Francis Thackeray [d], Francis Albarède [b]

[a] *UMR 5125 "PaléoEnvironnements et PaléobioSphère", CNRS, France, Université Lyon 1, Campus de la Doua, Bâtiment Géode, 69622 Villeurbanne Cedex, France*
[b] *UMR 5570 "Laboratoire de Sciences de la Terre", CNRS, France, Ecole Normale Supérieure de Lyon-Université Lyon 1, 46 Allée d'Italie, 69364 Lyon Cedex 7, France*
[c] *FRE 2960 "Laboratoire d'Anthropobiologie", CNRS, France, Université Toulouse 3, 39 Allées Jules Guesde, 31000 Toulouse, France*
[d] *Transvaal Museum, P.O. Box 413, Pretoria 0001, South Africa*

Received 25 February 2008; accepted in revised form 22 May 2008; available online 8 June 2008

Abstract

We present in this study results obtained with a laser-ablation coupled with both a quadrupole and a multi-collector ICPMS. The simultaneous *in situ* Sr/Ca and $^{87}Sr/^{86}Sr$ measurements along growth profiles in enamel allows the concomitant diet and migration patterns in mammals to be reconstructed. Aliquots of the powdered international standard NIST "SRM1400 Bone Ash" with certified Sr and Ca contents, was sintered at high pressure and temperature and was adopted as the reference material for external reproducibility and calibration of the results. A total of 145 coupled elemental and isotopic measurements of herbivores enamel from the Kruger National Park, South Africa, gives intra-tooth Sr/Ca and $^{87}Sr/^{86}Sr$ variations that are well larger than external reproducibility. Sr/Ca profiles systematically decrease from the dentine-enamel junction to the outer enamel whereas $^{87}Sr/^{86}Sr$ profiles exhibit variable patterns. Using a simple geometric model of hypsodont teeth growth, we demonstrate that a continuous recording of the $^{87}Sr/^{86}Sr$ variations can be reconstructed in the tooth length axis. This suggests that the mobility of a mammal can be reconstructed over a period of more than a year with a resolution of a ten of days, by sampling enamel along growth profiles. Our geometric model of hypsodont teeth growth predicts that an optimal distance between two successive profiles is equal to the enamel thickness. However, this model does not apply to the Sr/Ca signal which is likely to be altered during the enamel maturation stage due to differential maturation processes along enamel thickness. Here, the observed constant decreases of the Sr/Ca ratios in the ungulates of Kruger National Park suggests that they did not changed of diet, while some of them were migrating.

1. INTRODUCTION

In recent years, there has been a growing interest in the application of laser ablation inductively-coupled plasma mass spectrometry (LA-ICP-MS) to trace-element profiling of incrementally grown biological tissues such as corals (Munksgaard et al., 2004; Sinclair, 2005; Sinclair et al., 1998), shells (Christensen et al., 1995), otoliths (Woodhead et al., 2005; Clarke et al., 2007), and teeth (Ghazi et al., 2000; Hoffmann et al., 2000; Dolphin et al., 2005; Cucina et al., 2007). Tooth enamel receives a growing interest because it allows to reconstruct age-related changes during the lifetime of living and fossil humans (Dolphin et al., 2005; Humphrey et al., 2008; Richards et al., 2008).

Dental enamel is a heavily mineralized tissue which forms early in the lifetime of an animal and is not remodeled thereafter. As a result, the chemical variations of enamel are a function physiological states and environmental

* Corresponding author. Fax: +33 4 72 72 88 77.
E-mail address: Vincent.Balter@univ-lyon1.fr (V. Balter).

0016-7037/$ - see front matter © 2008 Elsevier Ltd. All rights reserved.
doi:10.1016/j.gca.2008.05.048

changes during tooth mineralization only. However, the pattern of enamel growth (i.e. mineralization schedule and tooth shape) controls the geometry of these variations. For instance, intra-tooth carbon and oxygen stable isotopes variations in fossil enamel, which are extensively used to reconstruct changes in ancient dietary habits and past climates (Fricke et al., 1998; Balasse, 2002; Zazzo et al., 2002), are known to depend on the micro-sampling strategy. This is due to the fact that the enamel maturation stage is a three-dimensional complex process which anisotropically damps the primary signal recorded at the enamel matrix deposition stage (Passey and Cerling, 2002; Balasse, 2003; Zazzo et al., 2005).

Of particular interest for ancient mammal dietary habits and migrations reconstructions, is the study of fossil enamel strontium/calcium ratio (Sr/Ca) (Sponheimer et al., 2005; Sponheimer and Lee-Thorp, 2006) and strontium stable isotope ratio ($^{87}Sr/^{86}Sr$) (Feranec et al., 2007; Muller et al., 2003; Sillen et al., 1998; Wright, 2005), respectively. On the one hand, the Sr/Ca ratio is a proxy of trophic level which is based on the constant discrimination of dietary Sr by mammals resulting in predictable lower Sr/Ca in consumer relative to its diet (Balter, 2004). While this picture has been clearly depicted for bone for fifty years since the pioneering works of Comar et al. (1956), the Sr/Ca patterning for enamel seems to be slightly different. On the basis of data on modern mammals from the Kruger National Park (South Africa), it appears that grazing herbivores have the highest Sr/Ca ratio, followed by browsing herbivores and carnivores (Sponheimer et al., 2005; Sponheimer and Lee-Thorp, 2006). On the other hand, because the abundances of the radiogenic ^{87}Sr isotope are determined after normalization of stable isotope variations to a reference $^{86}Sr/^{88}Sr$ ratio of 0.1194, the $^{87}Sr/^{86}Sr$ ratio is immune to biological and any other process down the trophic chain. Consequently, the $^{87}Sr/^{86}Sr$ of an animal ultimately reflects that of the bedrock on which it feeds (Hobson, 1999).

While this has never been clearly demonstrated, the validity of the Sr/Ca proxy implies that bone and tooth Sr and Ca are principally supplied by food and not by water. If the contrary was true, such proxy would not have existed because herbivores and carnivores of a trophic chain usually share the same water spots. Quantitatively, this can be easily demonstrated using allometric relationships between body mass (W, g) in one hand, and water intake (I_W, ml/h) or dry matter intake (I_{DM}, g/d) in the other hand, which are $I_W = 0.010\ W^{0.880}$ (Eq. 1) and $I_{DM} = 0.577\ W^{0.727}$ (Eq. 2), respectively (Adolph, 1949; Nagy, 1987). Compiled values of the literature give Sr concentration in plants (~50 ppm, values in Balter et al., 2001) three orders of magnitude higher than in rivers and meat (~50 ppb) (Li, 1982; Balter et al., 2001). For a given body mass, this gives that the Sr amount derived from plants and meat is higher than the Sr amount derived from water by two and five orders of magnitude, respectively.

Simultaneous analyses of Sr/Ca and $^{87}Sr/^{86}Sr$ ratios in fossil enamel should help to better describe the ecological behavior of extinct mammals, including hominids. For individuals within a species, this would allow to know whether diet variations were associated with migration or not and thus, whether this species was predominantly stenotopic (generalist, with a broad dietary spectrum and tolerant to a range of environments) or eurytopic (specialist, with a narrow dietary breadth and strong habitat preference). Here, we show that simultaneous Sr/Ca and $^{87}Sr/^{86}Sr$ analysis in enamel is feasible by coupling a quadrupole (Q-) and a multi-collector (MC-) ICPMS to a laser ablation. Accurate and reproducible results are obtained in spite of the relatively small pit size (~70 μm) and the moderate Sr concentration levels of the samples (~300 ppm). Moreover, we develop a geometric model that allows to reconstruct Sr isotopic variations throughout the growth of a hypsodont tooth.

2. MATERIAL

2.1. Teeth samples

The material is composed of four entire molars of three herbivores specimen (zebra, impala and sable antelope) from the Kruger National Park (KNP), South Africa. The three species considered are mobile animals. Zebras (*Equus burchellii*) graze over 50 different species of grasses mainly in open, short-grass savanna, whereas sable antelopes (*Hippotragus niger*) are specialized grazers feeding on foliage and herbs (Skinner and Smithers, 1990). Impalas (*Aepyceros melampus*) are intermediate feeders (Skinner and Smithers, 1990). The teeth of the zebra and sable antelope specimens are lower third molar (1132-M3 and 16999-M3, respectively) and the teeth of impala are lower second and third molars (16677-M2 and 16677-M3, respectively). Third molars are preferred to minimize contributions from suckling. The clean teeth samples were embedded in epoxy resin and sectioned longitudinally with a diamond wafering wheel saw. The resulting surfaces were gently polished manually on wet fine-grained sandpaper.

2.2. Solid apatite standards

Three international standards, two sedimentary apatite, SRM-120c ("Florida Phosphorite") and BRC-32 (Moroccan Phosphorite), and one biological apatite, SRM-1400 ("Bone Ash"), were used as references to assess the external reproducibility of the data. About 100 mg of these powdered samples were sintered at 2 GPa and 700 °C in a belt apparatus at the Centre des Hautes Pressions of the Claude Bernard Lyon1 University. In order to obtain clean and flat surfaces, the resulting sintered samples were manually abraded and polished using wet fine-grained sandpaper.

3. METHOD

3.1. Instrumental design

The Sr/Ca ratios were measured on the ThermoElement X7 quadrupole-ICPMS and the $^{87}Sr/^{86}Sr$ ratios on the Nu-HR (Nu-instrument) multicollector ICPMS of the Ecole Normale Supérieure in Lyon (ENSL). The laser is a 157 nm F_2/He excimer laser LPF202 of Lambda Physiks.

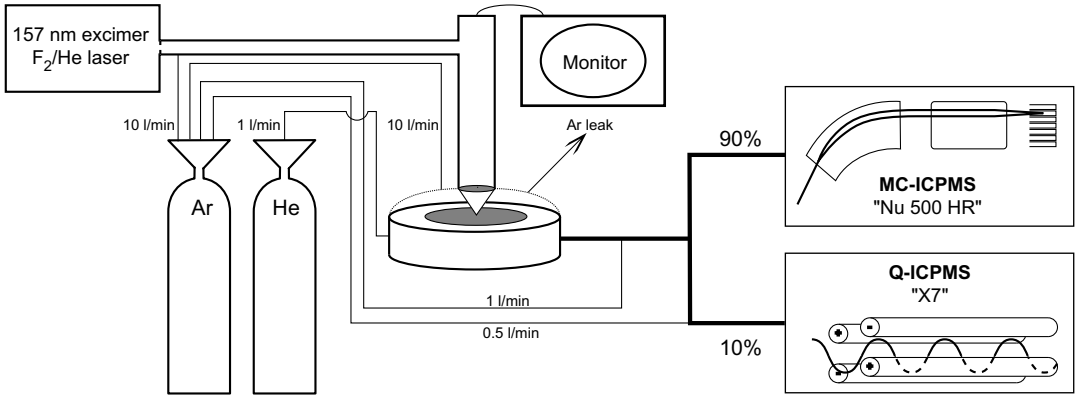

Fig. 1. Schematic of the laser ablation tandem quadrupole-multicollector ICPMS technique. The ablation cell is mounted on a motorized stage holder for X–Y–Z motion. The cell window as well as the convex lens are in CaF_2 (as indicated in gray). The ablation cell is surrounded by a skirt which is permanently purged by argon. Argon and helium flows are reported.

The three devices are coupled according to the Fig. 1. The laser ablation setup and the design of the sample chamber are described in detail in Telouk et al. (2003). The typical pit size is 70–100 μm (Fig. 2). For optimal sensitivity the installation was designed to direct about 90% of the ablated matter to the MC-ICPMS. As these conditions result in an inadequate argon flow to the Q-ICPMS, extra argon was added to overcome disequilibrium (Fig. 1).

3.2. Analytical conditions

Sr isotope data were obtained in static mode. Masses 88, 87, 86, 85, 84 and 83 were measured on Faraday cups. The isobaric interference of ^{87}Rb was corrected using the ^{85}Rb signal, which is extremely small (<1 mV), because Rb does not substitute to Ca in apatite. Krypton interferences at masses 84 and 86 (<1 mV) are corrected using ^{83}Kr. Sr and Ca concentrations were analyzed on the X7 using the ^{43}Ca, ^{44}Ca, and ^{88}Sr isotopes. All the results are expressed at the 95% confidence level (2σ). Blanks, which are typically lower than 1 mV, are measured with the laser off before each measurement run. The standard bone ash SRM-1400 which is certified to contain 250 ppm of Sr, produces typical signals of total Sr of about 250 mV on the MC-ICPMS. and 5×10^4 cps for the masse 88 on the Q-ICPMS. In order to calibrate the data obtained by laser ablation, the metal/Ca (*Me*/Ca) ratios of the three afore-mentioned international apatite standards were measured by wet chemistry and Q-ICPMS. The concentration ratios (Table 1) match the certified values (Fig. 3).

3.3. Geometry of hypsodont tooth growth

Here, we sampled enamel along growth prisms, i.e. along the track left by ameloblast cells (Fig. 2). This new strategy is expected to optimize the duration, as well as

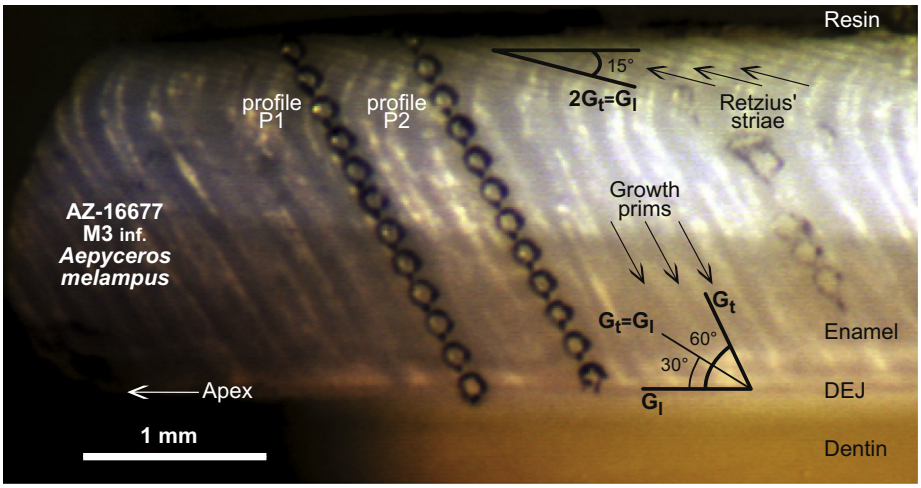

Fig. 2. Optical photograph of a polished section of tooth showing the different anatomical patterns discussed in the text, as well as the laser pits of the profiles P1 and P2 of the specimen AZ-16677 third molar. DEJ stands for dentino-enamel junction, G_l for growth in length, Gt for growth in thickness, respectively. The angle of the Retzius' lines and growth prisms with DEJ or outer enamel are reported. If the growth of the tooth is equal in length than in thickness, the Retzius' striae would be oriented with an angle of $60°/2 = 30°$ relative to the DEJ. Because this angle is approximately 15°, it is concluded that the tooth growths twice faster in length than in thickness.

Table 1
Measured (laser and solution) and certified metal/calcium (*Me*/Ca) values for three apatites international standards

x	*Me*/Ca (x10^3), BCR-32					*Me*/Ca (x10^3), SRM-1400			*Me*/Ca (x10^3), SRM-120c				
	Measured				Certified	Measured		Certified	Measured				Certified
	n	Laser	*n*	Solution		*n*	Laser		*n*	Laser	*n*	Solution	
Mg	*4*	3.4663 ± 2146	*21*	6.3283 ± 3558 (2.7)	6.5163 ± 1705 (0.2)	*3*	14.1295 ± 1.5257	17.9151 ± 3459 (1.7)	*2*	2.3477 ± 1628	17	5.4717 ± 2988 (4.3)	5.6234 ± 884 (0.0)
Mn	*4*	0.0822 ± 28	*4*	0.0447 ± 7 (3.9)	*0.0508 ± 30 (16.3)*				*2*	0.7093 ± 167	6	0.6243 ± 280 (0.6)	0.6093 ± 226 (6.1)
Sr	*4*	3.4986 ± 904	*19*	2.6726 ± 1727 (2.1)		*54*	1.2664 ± 773	0.6522 ± 185 (5.8)	*3*	3.9807 ± 1854	27	2.9345 ± 1403 (2.3)	2.4638[a] (1.9)
Ba	*4*	0.1927 ± 183	*15*	0.2880 ± 87 (4.5)		*54*	1.7309 ± 1461	0.6286 ± 263 (5.9)	*3*	0.1782 ± 749	27	0.2202 ± 70 (3.1)	
La	*2*	0.1071 ± 173	*3*	0.2914 ± 188 (9.9)					*2*	0.1153 ± 12	7	0.2695 ± 122 (8.6)	
Ce	*2*	0.0472 ± 63	*3*	0.0889 ± 22 (8.3)					*2*	0.2318 ± 31	7	0.3946 ± 150 (5.2)	
Nd	*2*	0.1432 ± 114	*3*	0.1793 ± 61 (3.4)					*2*	0.2206 ± 247	7	0.2320 ± 81 (1.6)	
Sm	*2*	0.0411 ± 10	*3*	0.0359 ± 13 (1.5)					*2*	0.0707 ± 164	7	0.0473 ± 16 (1.7)	
Eu	*2*	0.0166 ± 30	*3*	0.0098 ± 2 (2.0)					*2*	0.0240 ± 44	7	0.0110 ± 3 (5.2)	
Gd	*2*	0.1659 ± 137	*3*	0.0532 ± 11 (9.5)					*2*	0.2202 ± 723	7	*0.0543 ± 27 (12.2)*	
Tb	*2*	0.0104 ± 10	*3*	0.0076 ± 2 (0.9)					*2*	0.0140 ± 48	7	0.0079 ± 4 (2.4)	
Dy	*2*	0.0626 ± 18	*3*	0.0556 ± 17 (1.2)					*2*	0.0741 ± 143	7	0.0521 ± 18 (1.2)	
Ho	*2*	0.0150 ± 4	*3*	0.0135 ± 2 (2.8)					*2*	0.0155 ± 39	7	0.0116 ± 5 (0.7)	
Er	*2*	0.0512 ± 1	*3*	0.0445 ± 10 (1.2)					*2*	0.0533 ± 127	7	0.0353 ± 8 (1.6)	
Tm	*2*	0.0080 ± 0	*3*	0.0061 ± 1 (1.7)					*2*	0.0074 ± 13	6	0.0047 ± 1 (0.4)	
Yb	*2*	0.0678 ± 18	*3*	0.0409 ± 14 (2.7)					*2*	0.0634 ± 153	7	0.0301 ± 16 (5.2)	
Lu	*2*	0.0088 ± 8	*3*	0.0068 ± 2 (1.7)					*2*	0.0069 ± 16	7	0.0047 ± 2 (0.6)	
Pb	*4*	0.0228 ± 6	*4*	0.0096 ± 47 (6.2)	*0.0146*[a] *(22.4)*	*6*	0.0607 ± 85	*0.0238 ± 3 (19.9)*	*3*	0.0907 ± 44	7	0.0423 ± 60 (5.5)	*0.0811*[a] *(14.1)*
U	*4*	0.5948 ± 1306	*4*	0.3361 ± 158 (4.0)	0.3376[a] (8.2)				*3*	0.5723 ± 2897	7	0.3186 ± 163 (4.2)	0.3336 ± 25 (8.2)

Values in parenthesis are the residue (%) of the least-square regression between the laser and solution Me/Ca (Fig. 3A), and the laser and certified *Me*/*Ca* (Fig. 3B).
Values in italic are residue higher than 10%.
[a] Reported but not certified value.

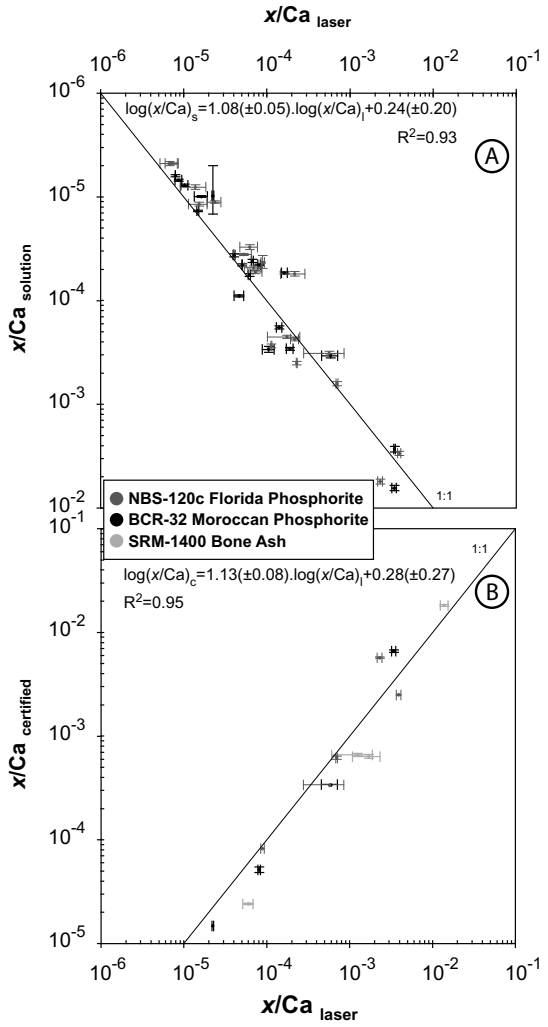

Fig. 3. (A) Plot of measured x/Ca ratio in solution and by laser ablation for three international apatite standards. The regression equation is reported. (B) Plot of certified x/Ca ratio and measured x/Ca ratio by laser ablation for three international apatite standards. The regression equation is reported. Data from Table 1.

the time resolution, of the enamel signal. Another important anatomical pattern of enamel is the Retzius' striae (Fig. 2), which are the ghosts of the advancing front of the forming enamel. From the angles made by the growth prisms and the Retzius' striae with the dentino-enamel junction (DEJ), ~60° and ~15°, respectively, teeth must have grown twice as fast in length as in thickness (Fig. 2). A sampling point located along a growth prism at a given distance from the DEJ, should therefore have the same signal as one located along the DEJ at twice this distance from the growth prism. In order to take these geometric constraints into account, all the profiles were positioned relative to each others with respect to the position of the first pit of the first profile (L^1_{abs}) along the DEJ according to the formula $(L^n_{abs} - L^1_{abs})/2 + L^1_{abs}$, L^n_{abs} being the position of the first pit along the DEJ of the n^{th} profile (Table 2).

4. RESULTS

The analyses on the solid SRM-1400 standard ($n = 14$), conducted under the normal coupled run conditions over two consecutive days, yielded an average Sr/Ca value of 0.001224 ± 0.000015, with an in-run precision of ± 0.000022 (Fig. 4). In comparison, Sr/Ca data ($n = 33$) collected over two years using LA-Q-ICPMS only, yielded an average of 0.001257 ± 0.000018 with an in-run precision of ± 0.000013 (Fig. 4). Coupled analysis of the solid SRM-1400 standard yield an average $^{87}Sr/^{86}Sr$ value of 0.71340 ± 0.00054 with an in-run precision of ± 0.00064 (Fig. 4). The $^{87}Sr/^{86}Sr$ value of this sample is not certified, but is similar to a TIMS result of 0.713104 ± 0.000019 reported by (Schweissing and Grupe, 2003). Taking into account the low Sr content (250 ppm) of the sample, the rather small size of the laser pit, and the small fraction (10%) of the sample directed to the Q-ICPMS, these results comparable favorably with those obtained using LA-Q-ICPMS (Sinclair et al., 1998; Hoffmann et al., 2000; Munksgaard et al., 2004), or LA-MC-ICPMS (Christensen et al., 1995; Bizzarro et al., 2003).

A total of 145 coupled analyses, distributed into 14 profiles of ~10 spots, yielded highly variable Sr/Ca and $^{87}Sr/^{86}Sr$ ratios (0.00430 ± 0.00336 and 0.7083 ± 0.0043, respectively). The Sr/Ca and $^{87}Sr/^{86}Sr$ variations given in Table 2 exceeds the external reproducibility by a factor of 30-500 for the Sr/Ca ratio and of 2-8 for the $^{87}Sr/^{86}Sr$ ratio. Additional LA-Q-ICPMS ($n = 178$) and LA-MC-ICPMS analyses ($n = 48$) give similar results, with variations larger by a factor of 30-500 and two for the Sr/Ca and $^{87}Sr/^{86}Sr$ ratios, respectively.

5. DISCUSSION

The geological substrates of the KNP (stretching over about 15,000 Km^2 between 22°30′S and 25°30′S and 31°00′E and 32°00′E) are mainly composed by >3 Ga years old archean gneisses which are intruded by granites of the Murchinson Sequence, and by the Lebombo Volcanic Group of the Karoo Sequence (Schutte, 1986). Intrusive, volcanic and sedimentary rocks represent 55%, 41% and 3%, respectively, of the total surface of KNP. Contemporaneous gneisses of the Kaapvaal Craton (Swaziland) and of the Zimbabwe Craton yield $^{87}Sr/^{86}Sr$ values of 0.7102 ± 0.0022 and 0.7108 ± 0.0050, respectively (Davies and Allsopp, 1976; Wilson et al., 1978). The granite of the Murchinson Sequence is represented at KNP by the Nelspruit Migmatite which has a $^{87}Sr/^{86}Sr$ values of 0.7114 (Davies and Allsopp, 1976). The Lebombo Volcanic Group is composed of several basalt types for which a global $^{87}Sr/^{86}Sr$ of 0.7056 ± 0.0007 is given by Sweeney et al. (1994). Although we did not analyze plants or soils samples from the KNP, the range of the $^{87}Sr/^{86}Sr$ values obtained in enamel (~0.704 to ~0.718; Table 2) well reflects the Sr isotope variability of the KNP geological substrates. Replacing our samples in this isotopic context allows to deduce that the sable antelope and the impala preferentially attended the western granitic area of KNP whereas the zebra was more regularly on the eastern basaltic part of KNP.

Table 2
Mean, standard deviation, maximum and minimum of the Sr/Ca and $^{87}Sr/^{86}Sr$ profiles measured by LA-QMC-ICPMS, or LA-Q-ICPMS and LA-MC-ICPMS

Sample ID	Profile ID	*n*	L_{abs}%[a]	L_{cor}%[b]	Tandem LA-QMC-ICPMS				LA-Q-ICPMS		LA-MC-ICPMS	
					Sr/Ca		$^{87}Sr/^{86}Sr$		Sr/Ca		$^{87}Sr/^{86}Sr$	
					Mean ± SD	Max.–Min.	Mean ± SD	Max.–Min.	Mean ± SD	Max.–Min.	Mean ± SD	Max.–Min.
16677-M2	QMC-M2-1	*12*	43	43	0.0079 ± 7	0.0087-0.0066	0.7068 ± 3	0.7074-0.7064				
	QMC-M2-2	*10*	72	58	0.0081 ± 15	0.0101-0.057	0.7066 ± 2	0.7070-0.7062				
	QMC-M2-3	*10*	90	66	0.0081 ± 11	0.0102-0.0062	0.7069 ± 3	0.7077-0.7066				
	Q-M2-P1	*14*	42	42					0.0077 ± 9	0.0088-0.0059		
	Q-M2-P2	*10*	72	59					0.0080 ± 16	0.0099-0.0050		
	Q-M2-P3	*9*	91	67					0.0082 ± 12	0.0105-0.0062		
16677-M3	QMC-M3-1	*11*	45	41	0.0072 ± 10	0.0091-0.0055	0.7066 ± 7	0.7080-0.7060				
	QMC-M3-2	*12*	80	56	0.0077 ± 17	0.0100-0.0051	0.7070 ± 6	0.7083-0.7064				
	QMC-M3-3	*11*	97	67	0.0077 ± 9	0.0087-0.0061	0.7068 ± 3	0.7073-0.7063				
	Q-M3-P1	*12*	37	37					0.0069 ± 8	0.0081-0.0052		
	Q-M3-P2	*11*	37	37					0.0069 ± 7	0.0078-0.0054		
	Q-M3-P3	*12*	78	57					0.0067 ± 18	0.0092-0.0044		
	Q-M3-P4	*11*	78	57					0.0067 ± 17	0.0089-0.0042		
	Q-M3-P5	*12*	96	66					0.0063 ± 7	0.0069-0.0043		
	Q-M3-P6	*12*	96	66					0.0067 ± 7	0.0072-0.0048		
	MC-P4	*13*	36	36							0.7062 ± 3	0.7069-0.7058
	MC-P2	*11*	76	56							0.7075 ± 4	0.7081-0.7068
	MC-P1	*13*	78	57							0.7073 ± 4	0.7079-0.7067
	MC-P3	*13*	93	65							0.7072 ± 5	0.7078-0.7065
16999-M3	QMC-1	*11*	12	12	0.00063 ± 12	0.00089-0.00052	0.7054 ± 13	0.7075-0.7036				
	QMC-3	*10*	28	20	0.00061 ± 11	0.00079-0.00047	0.7049 ± 11	0.7067-0.7032				
	QMC-4	*10*	66	39	0.00066 ± 8	0.00082-0.00054	0.7042 ± 6	0.7052-0.7030				
	QMC-5	*11*	88	50	0.00062 ± 13	0.00086-0.00045	0.7038 ± 6	0.7045-0.7026				
	Q-16999-P1	*12*	13	12					0.00061 ± 13	0.00092-0.00047		
	Q-16999-P2	*11*	29	21					0.00065 ± 16	0.00093-0.00042		
	Q-16999-P3	*11*	67	40					0.00064 ± 11	0.00086-0.00046		
	Q-16999-P4	*13*	89	51					0.00066 ± 13	0.00090-0.00048		
1132-M3	QMC-AZ4	*6*	65	66	0.0020 ± 2	0.0022-0.0017	0.7160 ± 7	0.7165-0.7146				
	QMC-AZ3	*11*	70	67	0.0025 ± 5	0.0034-0.0020	0.7160 ± 13	0.7184-0.7138				
	QMC-AZ2	*11*	77	74	0.0024 ± 5	0.0030-0.0018	0.7148 ± 11	0.7169-0.7128				
	QMC-AZ1	*9*	91	78	0.0019 ± 2	0.0021-0.0017	0.7142 ± 6	0.7156-0.7135				
	Q-AZ-P2	*9*	74	70					0.0021 ± 3	0.0027-0.0017		
	Q-AZ-P1	*11*	88	77					0.0019 ± 1	0.0020-0.0016		

[a] L_{abs} is the position of the first pit relative to the total length of the teeth.
[b] L_{cor} is the position of the first pit relative to the total length of the teeth, corrected for the differential growth rate between length and thickness, and normalized position of the first pit of the first profile.

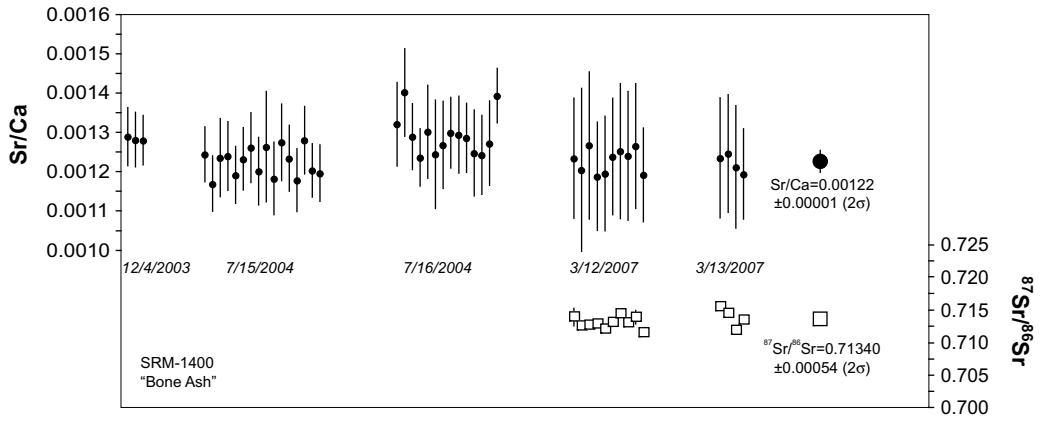

Fig. 4. Coupled Sr/Ca and $^{87}Sr/^{86}Sr$ measurements by LA-QMC-ICPMS of the international apatite standard SRM-1400 "Bone Ash". The date of the measurements is reported.

These conclusions are supported by the higher Sr isotope values found in ivory and bone of elephants living in the western part of KNP than living in the eastern one (van der Merwe et al., 1990; Vogel et al., 1990). The Sr/Ca values obtained in the present study are slightly lower than those reported by Sponheimer and Lee-Thorp (2006) on different species of mammals from the KNP. The small number of grazers and the absence of carnivore and browser in our samples does not allow to observe the Sr/Ca patterning revealed by Sponheimer and Lee-Thorp (2006).

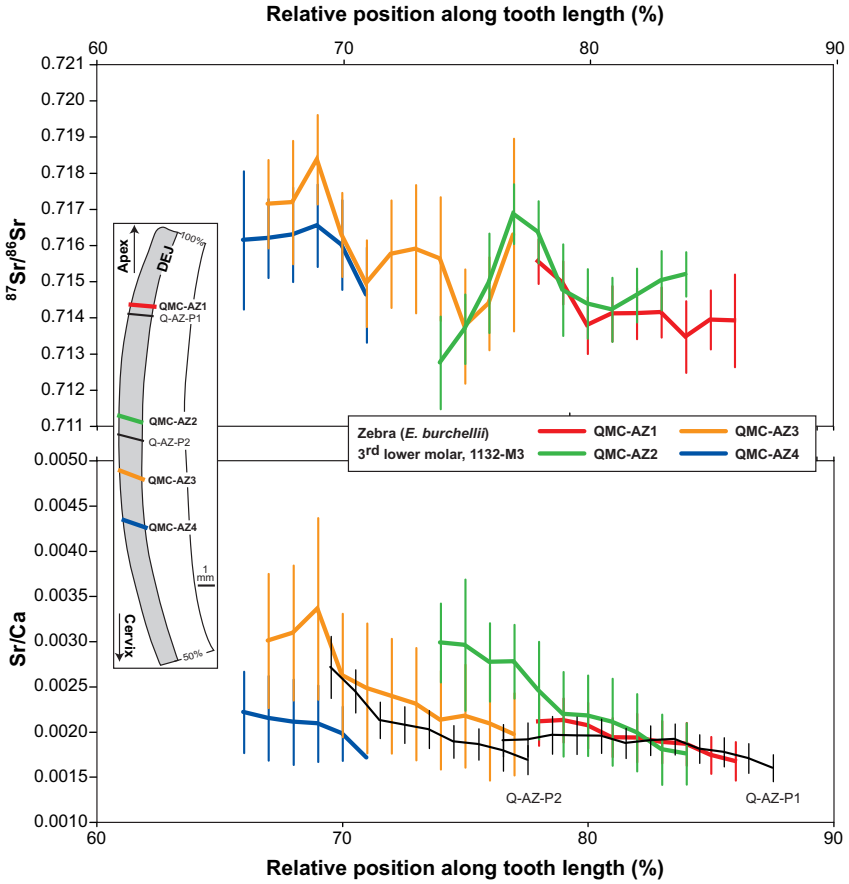

Fig. 5. Reconstructed Sr/Ca variations (lower panel) and $^{87}Sr/^{86}Sr$ variations (upper panel) along the length axis of a third lower molar of zebra (1132-M3). Black Sr/Ca profiles are additional LA-Q-ICPMS measurements. Data from Table 2.

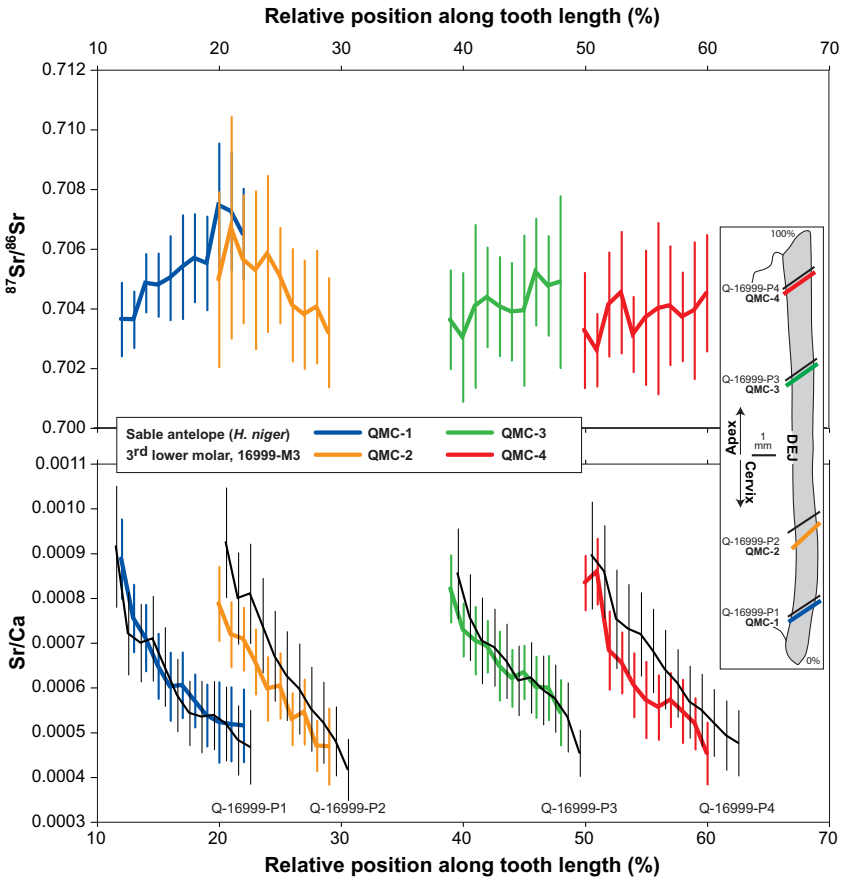

Fig. 6. Reconstructed Sr/Ca variations (lower panel) and $^{87}Sr/^{86}Sr$ variations (upper panel) along the length axis of a third lower molar of sable antelope (16999-M3). Black Sr/Ca profiles are additional LA-Q-ICPMS measurements. Data from Table 2.

The results are presented in Figs. 5–8. The Sr/Ca ratios systematically decrease from DEJ to the enamel surface (ES) whereas $^{87}Sr/^{86}Sr$ profiles exhibit fluctuating patterns. Most importantly, our assumptions about tooth growth geometry are validated by consistent $^{87}Sr/^{86}Sr$ profiles, which demonstrated that a continuous record of the $^{87}Sr/^{86}Sr$ variations can be reconstructed from piecewise analyses along the tooth length. The consistency of isotopic profiles is particularly visible in the case of the third molar of the impala (Fig. 8), for which the profiles MC-P4 and QMC-M3-1 match perfectly over 40–50% of the tooth length. The bump at about 67% present on four profiles (MC-P2, MC-P1, QMC-M3-2 and MC-P3) is particularly striking (Fig. 8). Although zebras and sable antelopes are free rangers (Skinner and Smithers, 1990) and thus should be characterized by variable enamel $^{87}Sr/^{86}Sr$ ratios, no clear isotopic series are observed for these animals, probably because of the low Sr concentration in their enamel and/or the lack of variation (Figs. 5 and 6). However, it must be pointed out that overlying profiles are consistent (profiles QMC-AZ3, QMC-AZ2 and QMC-AZ-1 at about 77% for the 1132-M3 tooth, Fig. 5; profiles QMC-1 and QMC-3 at about 20% for the 16999-M3 tooth, Fig. 6).

In contrast with the $^{87}Sr/^{86}Sr$ signal along the teeth length, the Sr/Ca signal varies by segments (e.g. Figs. 6 and 7). This observation can be explained easily if one supposes that the elemental and the isotopic ratios differentially bear the successive enamel mineralization phases, i.e. the matrix deposition stage and the maturation stage. During the matrix deposition stage, the Sr pool is incorporated into enamel from the body fluids with a partitioning relative to Ca most probably similar to bone (Balter, 2004; Sponheimer and Lee-Thorp, 2006). At this stage, the Sr isotope fractionation processes are considered negligible and the Sr isotope composition of enamel reflects that of diet. The Sr isotope composition is also unchanged during the maturation stage, while the Sr pool is modified relative to Ca, because of the active transcellular transport of Ca during this phase (Humphrey et al., 2008). From the histological point of view, the maturation process of hypsodont teeth, proceeds in successive fronts progressing inward or outward from DEJ (Suga, 1982). The completion of maturation is achieved with the mineralization of ES, this layer being the most highly mineralized (or Ca-enriched) of all the enamel layers. The observed recurring Sr/Ca ratio decreases from DEJ to ES can thus be explained by this mechanism. The recent

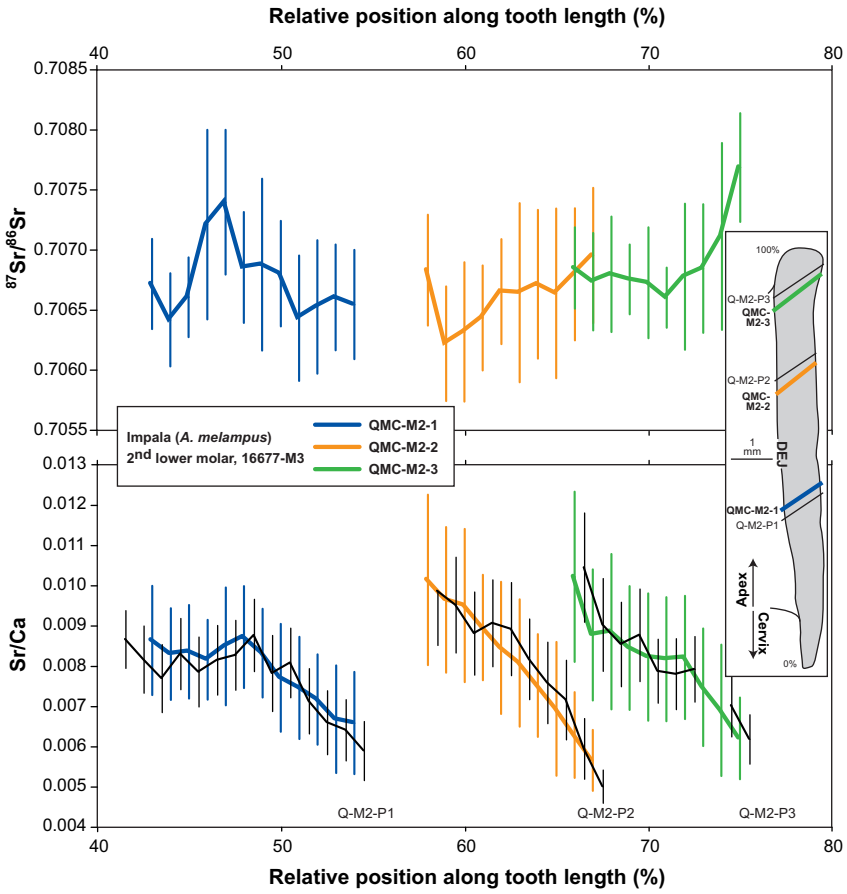

Fig. 7. Reconstructed Sr/Ca variations (lower panel) and $^{87}Sr/^{86}Sr$ variations (upper panel) along the length axis of a second lower molar of impala (16677-M2). Black Sr/Ca profiles are additional LA-Q-ICPMS measurements. Data from Table 2.

data of Humphrey et al. (2008) on Sr/Ca in enamel of children of known dietary history fully support our conclusions. In this study, the decrease of the Sr/Ca ratio from DEJ to ES is blatant in children who were fully fed from birth with infant formula diet, a result which unambiguously demonstrates that the Sr/Ca decrease is not associated with changing diet. Here, the observed Sr/Ca ratios decreases in the ungulates of KNP imply that they did not changed of diet, while some of them were migrating.

These results have several implications. First, the Sr/Ca intra-tooth variability should be more extended in the thickness than in the length of hypsodont teeth. Thus, care must be taken when sampling enamel for Sr/Ca bulk analysis (Sponheimer et al., 2005). For such studies, we recommend to drill enamel across its full thickness, the direction of the sampling relative to the tooth axis being of no matter. Second, the intra-tooth $^{87}Sr/^{86}Sr$ variability suggests that a sampling strategy based on profiles each separated with a distance equal to twice the thickness of enamel, should minimize the overlap between two successive profiles. For example, a typical bovid molar of 50 mm long with an enamel thickness of one mm, will allow to perform about 25 profiles, corresponding to a resolution of about two weeks given that the molar tooth is formed in roughly one year.

6. CONCLUSION

For the first time, elemental and isotopic results obtained with a laser-ablation coupled with a quadrupole and a multi-collector ICPMS, are presented. Here, this technique allows to measure the Sr/Ca and the $^{87}Sr/^{86}Sr$ ratios along growth profiles in recent tooth enamel in order to decipher diet and migration patterns in mammals. The calibration method involves several solid apatites that were sintered from powdered international standards. Repeated analysis of the solid SRM-1400 standard yielded results that are comparable with reported values on LA-Q-ICPMS or LA-MC-ICPMS. In one hand, intra-tooth Sr/Ca variations reveal that the Sr/Ca profiles systematically decrease from DEJ to ES reflecting most probably the progressive closure of the enamel during the maturation stage. In the other hand, intra-tooth $^{87}Sr/^{86}Sr$ variations show varying patterns suggesting that this isotopic ratio is insensitive to enamel maturation. Lastly, we demonstrate using a simple geometric model of tooth growth that a continuous recording of the $^{87}Sr/^{86}Sr$ variations can be reconstructed using the whole tooth length. This suggests that the mobility of a mammal can be reconstructed over a period of more than a year with a resolution of ten of days, by sampling the enamel thickness at several tooth length intervals.

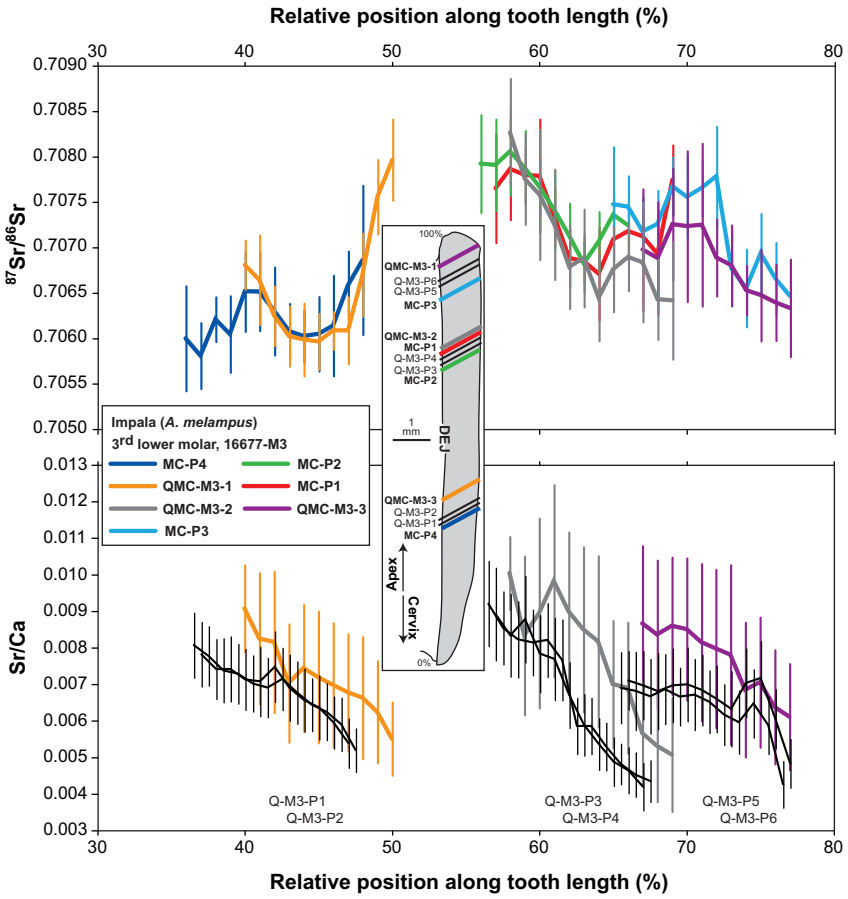

Fig. 8. Reconstructed Sr/Ca variations (lower panel) and $^{87}Sr/^{86}Sr$ variations (upper panel) along the length axis of a third lower molar of impala (16677-M3). Black Sr/Ca profiles are additional LA-Q-ICPMS measurements. Data from Table 2.

ACKNOWLEDGMENTS

The authors are grateful to Teresa Kearney for facilitating the access to the mammal collection of the Transvaal Museum, and Klervia Jaouen for assistance during one session of laser ablation. We also thank three anonymous reviewers for their helpful comments. This project was funded by the French INSU program ECLIPSE 2.

REFERENCES

Adolph E. F. (1949) Quantitative relations in the physiological constitutions of mammals. *Science* **109**, 579–585.

Balasse M. (2002) Reconstructing dietary and environmental history from enamel isotopic analysis: time resolution of intra-tooth sequential sampling. *Int. J. Osteoarchaeol.* **12**, 155–165.

Balasse M. (2003) Potential biases in sampling design and interpretation of intra-tooth isotope analysis. *Int. J. Osteoarchaeol.* **13**, 3–10.

Balter V. (2004) Allometric constraints on Sr/Ca and Ba/Ca partitioning in terrestrial mammalian trophic chains. *Oecologia* **139**, 83–88.

Balter V., Person A., Labourdette N., Drucker D., Renard M. and Vandermeersch B. (2001) Were Neandertalians essentially carnivores? Sr and Ba preliminary results of the mammalian palaeobiocoenosis of Saint-Cesaire. *C. R. Geosci.* **332**, 59–65.

Bizzarro M., Simonetti A., Stevenson R. and Kurszlaukis S. (2003) In situ $^{87}Sr/^{86}Sr$ investigation of igneous apatites and carbonates using laser-ablation MC-ICP-MS. *Geochim. Cosmochim. Acta* **67**, 289–302.

Christensen J. N., Halliday A. N., Lee D.-C. and Hall C. M. (1995) In situ Sr isotopic analysis by laser ablation Earth. *Planet. Sci. Lett.* **136**, 79–85.

Clarke A. D., Telmer K. H. and Mark Shrimpton J. (2007) Elemental analysis of otoliths, fin rays and scales: a comparison of bony structures to provide population and life-history information for the Arctic grayling (Thymallus arcticus). *Ecol. Freshw. Fish* **16**, 354–361.

Comar C. L., Russell L., Wasserman R. H. and Nold N. L. (1956) Strontium-calcium discrimination factors in the rat. *Proc. Soc. Exp. Med. Biol.* **92**, 859–863.

Cucina A., Dudgeon J. and Neff H. (2007) Methodological strategy for the analysis of human dental enamel by LA-ICP-MS. *J. Archaeol. Sci.* **34**, 1884–1888.

Davies R. D. and Allsopp H. L. (1976) Strontium isotopic evidence relating to the evolution of the lower Precambrian granitic crust in Swaziland. *Geology* **4**, 553–556.

Dolphin A. E., Goodman A. H. and Dulasiri D. A. (2005) Variation in elemental intensities among teeth and between pre- and postnatal regions of enamel. *Am. J. Phys. Anthropol.* **128**, 878–888.

Feranec R., Hadly E. and Paytan A. (2007) Determining landscape use of Holocene mammals using strontium isotopes. *Oecologia* **153**, 943–950.

Fricke H. C., Clyde W. C. and O'Neil J. R. (1998) Intra-tooth variations in [delta]18O (PO4) of mammalian tooth enamel as a record of seasonal variations in continental climate variables. *Geochim. Cosmochim. Acta* **62**, 1839–1850.

Ghazi A. M., Shuttleworth S., Angulo S. J. and Pashley D. H. (2000) New applications for laser ablation high resolution ICPMS (LA-HR-ICP-MS): quantitative measurements of gallium diffusion across human root dentin J. *Anal. At. Spectrom.* **15**, 1335–1341.

Hobson K. A. (1999) Tracing origins and migration of wildlife using stable isotopes: a review. *Oecologia* **120**, 314–326.

Hoffmann E., Stephanowitz H., Ullrich E., Skole J., Lüdke C. and Hoffmann B. (2000) Investigation of mercury migration in human teeth using spatially resolved analysis by laser ablation-ICP-MS J. *Anal. At. Spectrom.* **15**, 663–667.

Humphrey L. T., Dean M. C., Jeffries T. E. and Penn M. (2008) Unlocking evidence of early diet from tooth enamel. *Proc. Natl. Acad. Sci.* **105**, 6834–6839.

Li Y.-H. (1982) A brief discussion on the mean oceanic residence time of elements. *Geochim. Cosmochim. Acta* **46**, 2671–2675.

Muller W., Fricke H., Halliday A. N., McCulloch M. T. and Wartho J.-A. (2003) Origin and migration of the Alpine Iceman. *Science* **302**, 862–866.

Munksgaard N. C., Antwertinger Y. and Parry D. L. (2004) Laser ablation ICP-MS analysis of Faviidae corals for environmental monitoring of a tropical estuary. *Environ. Chem.* **1**, 188–196.

Nagy K. A. (1987) Field metabolic rate and food requirement scaling in mammals and birds. *Ecol. Monogr.* **57**, 111–128.

Passey B. H. and Cerling T. E. (2002) Tooth enamel mineralization in ungulates: implications for recovering a primary isotopic time-series. *Geochim. Cosmochim. Acta* **66**, 3225–3234.

Richards M., Harvati K., Grimes V., Smith C., Smith T., Hublin J.-J., Karkanas P. and Panagopoulou E. (2008) Strontium isotope evidence of Neanderthal mobility at the site of Lakonis, Greece using laser-ablation PIMMS. *J. Archaeol. Sci.* **35**, 1251–1256.

Schutte I. C. (1986) The general geology of the Kruger National Park. *Koedoe* **29**, 13–37.

Schweissing M. M. and Grupe G. (2003) Stable strontium isotopes in human teeth and bone: a key to migration events of the late Roman period in Bavaria. *J. Archaeol. Sci.* **30**, 1373–1383.

Sillen A., Hall G., Richardson S. and Armstrong R. (1998) $^{87}Sr/^{86}Sr$ ratios in modern and fossil food-webs of the Sterkfontein Valley: implications for early hominid habitat preference. *Geochim. Cosmochim. Acta* **62**, 2463–2473.

Sinclair D. J. (2005) Correlated trace element "vital effects in tropical corals: a new geochemical tool for probing biomineralization. *Geochim. Cosmochim. Acta* **69**, 3265–3284.

Sinclair D. J., Kinsley L. P. J. and McCulloch M. T. (1998) High resolution analysis of trace elements in corals by laser ablation ICP-MS. *Geochim. Cosmochim. Acta* **62**, 1889–1901.

Skinner J. and Smithers R. (1990) *Mammals of the Southern African Subregion*, 2nd ed. University of Pretoria, Pretoria.

Sponheimer M., de Ruiter D., Lee-Thorp J. and Spath A. (2005) Sr/Ca and early hominin diets revisited: new data from modern and fossil tooth enamel. *J. Hum. Evol.* **48**, 147–156.

Sponheimer M. and Lee-Thorp J. A. (2006) Enamel diagenesis at South African Australopith sites: implications for paleoecological reconstruction with trace elements. *Geochim. Cosmochim. Acta* **70**, 1644–1654.

Suga S. (1982) Progressive mineralization pattern of developing enamel during the maturation stage. *J. Dent. Res.* **61**, 1532–1542.

Sweeney R. J., Duncan A. R. and Erlank A. J. (1994) Geochemistry and petrogenesis of Central Lebombo Basalts of the Karoo Igneous Province. *J. Petrol.* **35**, 95–125.

Telouk P., Rose-Koga E. and Albarede F. (2003) Preliminary results from a new 157nm laser ablation ICP-MS instrument: new opportunities in the analysis of solid samples. *Geostandard. Newslett.* **27**, 5–11.

van der Merwe N. J., Lee-Thorp J. A., Thackeray J. F., Hall-Martin A., Kruger F. J., Coetzee H., Bell R. H. V. and Lindeque M. (1990) Source-area determination of elephant ivory by isotopic analysis. *Nature* **346**, 744–746.

Vogel J. C., Eglington B. and Auret J. M. (1990) Isotope fingerprints in elephant bone and ivory. *Nature* **346**, 747–749.

Wilson J. F., Bickle M. J., Hawkesworth C. J., Martin A., Nisbet E. G. and Orpen J. L. (1978) Granite-greenstone terrains of the Rhodesian Archaean craton. *Nature* **271**, 23–27.

Woodhead J., Swearer S., Hergt J. and Maas R. (2005) In situ Sr-isotope analysis of carbonates by LA-MC-ICP-MS: interference corrections, high spatial resolution and an example from otolith studies. *J. Anal. At. Spectrom.* **20**, 22–27.

Wright L. E. (2005) Identifying immigrants to Tikal, Guatemala: defining local variability in strontium isotope ratios of human tooth enamel. *J. Archaeol. Sci.* **32**, 555–566.

Zazzo A., Balasse M. and Patterson W. P. (2005) High-resolution [delta]13C intratooth profiles in bovine enamel: implications for mineralization pattern and isotopic attenuation. *Geochim. Cosmochim. Acta* **69**, 3631–3642.

Zazzo A., Mariotti A., Lecuyer C. and Heintz E. (2002) Intra-tooth isotope variations in late Miocene bovid enamel from Afghanistan: paleobiological, taphonomic, and climatic implications. *Paleogeogr. Paleoclimatol. Paleoecol.* **186**, 145–161.

Associate editor: Miryam Bar-Matthews